JOURNAL OF Materials CHEMISTRY

The continuous hydrothermal synthesis of nano-particulate ferrites in near critical and supercritical water

Albertina Cabañas* and Martyn Poliakoff*

School of Chemistry, The University of Nottingham, University Park, Nottingham, UK NG7 2RD. E-mail: url: http://www.nottingham.ac.uk/supercritical/. E-mail: Martyn.Poliakoff@nottingham.ac.uk

Received 24th November 2000, Accepted 16th February 2001
First published as an Advance Article on the web 28th March 2001

Magnetic spinel type oxides such as magnetite, Fe_3O_4, cobalt, nickel, and zinc ferrites, MFe_2O_4 (M = Co, Ni, Zn) and the mixed nickel and cobalt ferrite, $Ni_xCo_{1-x}Fe_2O_4$ have been synthesised continuously by the hydrolysis and simultaneous oxidation of mixtures of Fe(II) acetate and different M(II) acetates in near-critical and supercritical water using a flow reactor. The materials have been characterised by powder X-ray diffraction (PXD) and, in selected cases, by transmission electron microscopy (TEM). The bulk composition of the samples was determined by Atomic Absorption analysis (AA). Additionally, Energy-dispersive Detection X-ray analysis (EDX) was carried out on some of the samples. TEM pictures showed a "bimodal" particle size distribution: small particles of *ca.* 10 nm and larger particles of up to 100 nm, both of which are highly crystalline. Possible reaction mechanisms are discussed, which may be responsible for the observed morphology. The effects of temperature and residence time on the reaction have been studied.

Introduction

Pure magnetite, Fe_3O_4, and ferrites have been used in a variety of materials including magnetic pigments in recording media and magnetic fluids for the storage and/or retrieval of information, as well as catalysts.[1,2] There is much interest in the production of nanoparticulate magnetic materials, as reducing the particle size will allow miniaturisation of the size of the device.[3]

The magnetic properties of the ferrites, MFe_2O_4, depend on the cation configuration of the spinel lattice. In the above formula, M represents a divalent metal ion such as Fe^{2+}, Mn^{2+}, Co^{2+}, Ni^{2+}, Cu^{2+} or Zn^{2+}, but a combination of these cations is also possible and in this case we refer to them as a solid solution of two ferrites, mixed crystal or, in general terms, as a mixed ferrite. The degree of inversion in the spinel lattice depends on the ionic radius, on the electrostatic energy and, principally, on the electronic configuration of the cations and the relative stabilisation energies of these in the tetrahedral and octahedral fields. Among the ferrites studied in this work, magnetite, Fe_3O_4, and the nickel and cobalt ferrites, $NiFe_2O_4$ and $CoFe_2O_4$, are usually inverse spinels whilst zinc ferrite, $ZnFe_2O_4$, is a normal spinel.[4] However, the detailed cation distribution often depends on the sample preparation.[2] In addition, for a given cation distribution, the magnetic properties depend strongly on the microstructural features such as morphology, crystallite size and porosity. A large particle is composed of many small magnetic domains, where all of the spins are orientated in the same direction. Different domains have different magnetic vectors, but the overall vector points in one direction giving an overall magnetic moment. Nanoparticles, which are not large enough to support the formation of boundaries between magnetic domains, may behave as single magnets when the domain size is as large as the particle.[3]

These oxides are routinely synthesised by conventional solid state reactions at temperatures[4] close to 1400 °C but, at such a high temperature, particles sinter and thus lose their fine particulate nature. Alternatively, a number of wet methods including co-precipitation,[1] sol–gel,[5] microemulsions,[6] oxidation techniques[7] and hydrothermal synthesis (mainly in batch)[8,9] have been shown to overcome these problems with differing degrees of success. However, some of these methods are non-environmentally friendly. Sol–gel and microemulsion techniques involve the use of large amounts of organic solvents or the addition of surfactants to the reaction medium. In co-precipitation, the pH of a metal salt solution is raised by adding a base in order to precipitate the hydroxides, which requires a strict control of the pH and the stirring rate. Besides, in most of these cases, the materials produced require further ageing, calcination or hydrothermal treatment to allow dehydration and to become more crystalline.

Hydrothermal synthesis has been carried out since the end of the 19th century,[10,11] mainly in the production of synthetic minerals to imitate natural geothermal processes. In modern terms, near-critical (nc) and supercritical (sc) water have been used as reaction media for the synthesis of highly crystalline metal oxides.[11–14] Haematite,[15–17] magnetite[3,15,16,18] and different ferrites[2,3,8,9,19,20] have been previously produced hydrothermally. However, except for the reports of Adschiri *et al.* concerning the synthesis of iron oxides[15,16] and barium hexaferrite particles[20] and the recent communication of Holm and Teja[3] of the synthesis of different spinel iron oxides, all these experiments have been carried out in batch reactors where the experimental conditions are sometimes poorly defined.[11] Most of these preparations involve a combination of co-precipitation and hydrothermal synthesis[3,9,20] to precipitate the corresponding hydroxides by the addition of bases. These hydroxides are then subjected to hydrothermal treatment in order to dehydrate them and achieve the desired degree of crystallinity.

An ideal process should be environmentally-friendly, requiring neither addition of solvents nor chemicals to the reaction medium, and should involve the lowest possible reaction temperature compatible with the desired product. The synthesis should be as simple as possible and a fast and continuous process would be preferred. Our aim is to produce singe phase nano-particulate and crystalline materials and, if possible, to control the morphology of the product by changing the experimental conditions.

We have recently reported a one-step synthesis of $Ce_{1-x}Zr_xO_2$ solid solutions ($x = 0$ to 1) in near-critical water.[21,22] By using a flow reactor, we were able to produce

 DOI: 10.1039/b009428p

continuously single phase crystalline nano-particulate $Ce_xZr_{1-x}O_2$ oxides. The higher self-dissociation constant and lower dielectric constant of water under near-critical conditions allows hydrolysis of the metal salts to occur without addition of base. This is in contrast with the literature syntheses of heterometallic oxides under flow conditions[3,20] where, prior to the hydrothermal treatment, co-precipitation of the hydroxides is necessary by adding a base. The lower dielectric constant in ncH_2O and scH_2O is the driving force inducing super-saturation and precipitation of small particles of metal hydroxides, which undergo fast dehydration. As a result, nano-particulate, highly crystalline materials are obtained. In our experience, flow reactors seem especially suitable for the synthesis of heterometallic oxides.[21,22] On the other hand, preliminary batch experiments on the hydrolysis of Fe(II) acetate, $Fe(Ac)_2$, in scH_2O showed the formation of magnetite, Fe_3O_4.[14] These observations encouraged us to investigate the synthesis of a range of metal ferrites by using mixtures of metal(II) acetate precursors in a scH_2O flow reactor.

Experimental

Flow experiments

All experiments were conducted using a small flow reactor built and designed in Nottingham (Fig. 1).[21] A summary of the experiments and experimental conditions is given in Tables 1 and 2. The reactor, tubing and different parts of the equipment were all made of 316 Swagelok stainless steel. Two Gilson pumps (P) (models 302 and 303) were used to bring into contact, respectively, an aqueous solution of metal acetates and a hot water stream previously heated up to 450 °C by a pre-heater (PH) (different temperatures are required for the different experiments). Flow rates of 5 and 10 mL min^{-1} were used for the metal and water streams, respectively. At the mixing point (X), the temperature, T_{mix}, was kept between 200 and 345 °C depending on the experiment. Downstream of the mixing point, a vertical tube reactor (7 cm^3 volume) was heated by a small electric furnace (H). The temperature of the reactor, T_{rea}, was kept constant at 200, 300 or 400 °C. After the reactor, the mixture was quenched immediately by water cooling (C). The mixture was then passed through a 7 μm filter (F) (to remove any large aggregates) and the back-pressure regulator (BPR), and it was collected as a suspension. The pressure was kept constant at 25 MPa. If it is assumed that the density of the reaction mixture is the same as that of pure water[23] under these conditions, the residence time in the reactor was between 2 and 25 seconds (see Table 3). When possible, the suspended products were separated from the aqueous phase by decantation and/or centrifugation and the solids were dried at

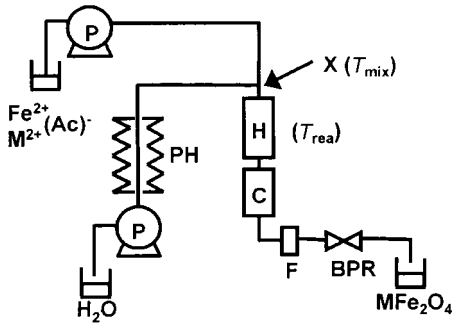

Fig. 1 Schematic diagram of the flow reactor used in the synthesis of ferrites in nc- and scH_2O. The parts are labelled as follows: (P) pump, (PH) pre-heater, (X) mixing point, (H) heater, (C) cooling, (F) filter, (BPR) back-pressure regulator. T_{mix} and T_{rea} are the temperatures at the mixing point and reactor, respectively. ***Safety**: These experiments involve high pressures and high temperatures, they should therefore be approached with caution.*

Table 1 Summary of the experiments on the decomposition of pure $Fe(Ac)_2$ in nc- and scH_2O: experimental conditions, identified products and particle size (PXD), and carbon content in the samples (%C)

Run	T_{mix}/°C	T_{rea}/°C	P/MPa	Products by PXD	Size[a]/nm	%C
1	200	200	25	Fe_3O_4 Fe (vw)	61	9.2
2	300	300	25	Fe_3O_4 Fe (w)	40	11.0
3	345	400	25	Fe_3O_4 Fe	92	1.0
Batch[b]		380	33	Fe_3O_4	158	5.6

[a]By using the Scherrer equation for the (440) reflection of Fe_3O_4. [b]Batch experiments: Reactions were carried out in a stainless steel 3.3 ml reactor for 1 hour following the procedure described by Boix and Poliakoff.[27] w weak; vw very weak.

100 °C. When centrifugation did not result in separation (due to the small particle size of the materials), some water was removed from the suspension using a rotary evaporator. The remaining solution containing the metal oxide was then dried in an oven at 100 °C.

Materials and method

$Fe(Ac)_2$, $Ni(Ac)_2{\cdot}4H_2O$, $Co(Ac)_2{\cdot}4H_2O$ and $Zn(Ac)_2{\cdot}2H_2O$ (Aldrich) were used without further purification. All experiments were conducted using HPLC grade triply distilled water (BDH). The water was degassed by bubbling N_2. However, the experimental procedure makes it difficult to keep the reaction medium absolutely free of O_2 and low concentrations of O_2 may have existed in solution. Metal salt solutions were prepared by dissolving $Fe(Ac)_2$ or a mixture of the corresponding metal acetates in the appropriate ratio in water. In all cases, the concentration of the metals in solution was 0.1 M. For the single ferrites, the ratio of $Fe(Ac)_2$ to the different metal acetates was 2 : 1, except for experiment 6 (Table 2) where a mixture of $Fe(Ac)_2$ and $Co(Ac)_2$ in a 1 : 1 ratio was used. For the nickel and cobalt mixed ferrite, the ratio of $Fe(Ac)_2$ to $Co(Ac)_2$ and $Ni(Ac)_2$ was 4 : 1 in both cases. Fresh solutions were prepared immediately prior to use, to avoid oxidation of Fe(II) by atmospheric O_2. The starting solutions were also degassed by bubbling N_2 through them.

All products were characterised by Powder X-ray Diffraction (PXD) and, in selected cases, by Transmission Electron Microscopy (TEM). The reaction yields of the hydrolysis products of pure $Ni(Ac)_2$ and $Co(Ac)_2$ were estimated by UV-vis spectroscopy. The relative amounts of the different metals in the bulk ferrites were determined by Atomic Absorption (AA). For some of the samples, the local relative amounts of the different metals were determined by Energy-dispersive Detection X-ray analysis (EDX). Samples were sent for C, H, N microanalysis. FTIR spectra of the powdered materials were recorded as KBr disks on a Nicolet Avatar instrument.

PXD data were collected using a Phillips EXPERT θ–2θ diffractometer with Cu K_α radiation. The sample was loaded onto an indented glass plate and scans were typically taken for 2 h over a 2θ range of 20–80°. The PC IDENTIFY program was used to assess the purity of the powders by comparison to the JCPDS database (card numbers in parentheses). The APD program was used to estimate the size of the particles in the sample by application of the Scherrer equation to the PXD line-widths of the different reflections (PC IDENTIFY and APD are part of the Phillips diffraction software package).

Transmission Electron Micrograph (TEM) pictures were obtained using a JEOL JEM-2000FXII TEM electron microscope operating at 200 KeV by placing one drop of a methanol/powder suspension on a 3.05 mm diameter copper mesh (300 lines per inch mesh), which was then dried in air. Metal analysis

Table 2 Summary of the experiments on the decomposition of mixtures of $Fe(Ac)_2$ and $Co(Ac)_2$, $Ni(Ac)_2$ and $Zn(Ac)_2$ in nc- and scH_2O: experimental conditions, identified products and particle size (PXD), ratio of the different metals by AA and carbon content in the samples (%C)

Run	T_{mix}/°C	T_{rea}/°C	P/MPa	Products by PXD	Size[a]/nm	AA	%C
Iron + cobalt starting $Fe^{2+}:Co^{2+}$ 2:1						$Fe^{2+}:Co^{2+}$	
4	205	200	25	$CoFe_2O_4$	39	2:0.93	16.0
5	300	300	25	$CoFe_2O_4$	58	2:1.00	3.9
6[b]	300	300	25	$CoFe_2O_4$ + CoO (vw)	57	2:1.87	15.3
7	335	400	25	$CoFe_2O_4$	72	2:0.81	5.2
Iron + nickel starting $Fe^{2+}:Ni^{2+}$ 2:1						$Fe^{2+}:Ni^{2}$	
8	190	200	25	$NiFe_2O_4$ Ni (w)	38	2:1.09	6.4
9	300	300	25	$NiFe_2O_4$	28	2:1.02	5.0
10	330	400	25	$NiFe_2O_4$ Ni (vw)	43	2:0.91	3.5
Iron + cobalt + nickel starting $Fe^{2+}:Co^{2+}:Ni^{2+}$ 2:0.5:0.5						$Fe^{2+}:Co^{2+}:Ni^{2+}$	
11	200	200	25	$Ni_xCo_{1-x}Fe_2O_4$ Ni (w)	29	2:0.54:0.81	9.5
12	315	300	25	$Ni_xCo_{1-x}Fe_2O_4$	42	2:0.47:0.61	6.7
13	330	400	25	$Ni_xCo_{1-x}Fe_2O_4$	23	4:0.53:0.62	10.1
Iron + zinc starting $Fe^{2+}:Zn^{2+}$ 2:1						$Fe^{2+}:Zn^{2+}$	
14	205	200	25	"$ZnFe_2O_4$" Fe (vw) Fe_3O_4 (vw)	47	2:0.68	4.7
15	300	300	25	"$ZnFe_2O_4$" Fe (vw) Fe_3O_4 (vw)	64	2:0.73	5.1
16	315	400	25	"$ZnFe_2O_4$" Fe (w) Fe_3O_4 (vw)	105	2:0.66	4.0

[a]By using the Scherrer equation for the (440) reflection of the spinel structure. [b]Starting Fe:Co ratio 1:1. w weak; vw very weak.

was carried out with a Noran Series II EDX system attached to the electron microscope.

For the hydrolysis of pure $Co(Ac)_2$ and $Ni(Ac)_2$, the reactions yields were estimated using an HP 8453 UV-vis spectrometer, by comparison of the absorption of the starting and final solutions (after the products settled). Elemental analyses were performed at Nottingham by the micro-analytical service (School of Chemistry). A Perkin-Elmer spectrophotometer model 603 in the flame absorption model was employed for the Atomic Absorption analyses (AA). Solutions for analysis were prepared by dissolving the samples in concentrated HCl and diluting them to the required concentrations. For the nickel ferrite and the mixed cobalt and nickel ferrite samples, standards containing iron and nickel at the ratio of the experiments (2:1 and 4:1, respectively) were prepared to overcome the interference of both metals. Nevertheless, when nickel and iron were both present in the material, the uncertainty in the determination of the metal ratio was larger.

Results

The experimental results are summarised in Tables 1 and 2, where the conditions of the experiments as well as the reaction products identified by PXD are indicated. Table 1 shows the experiments carried out with pure $Fe(Ac)_2$. It is clear that the partially oxidised iron oxide, Fe_3O_4, can be obtained by hydrothermal reaction of $Fe(Ac)_2$ solutions. As discussed later, oxidation of the Fe(II) species is thermodynamically possible in water. Table 2 summarises the experiments conducted with mixtures of $Fe(Ac)_2$ and at least one of the Co(II), Ni(II) and Zn(II) acetates. Under these conditions, oxidation of Fe(II) species still takes place and the corresponding metal ferrites, MFe_2O_4, are obtained. Depending on the particular metal, small amounts of different by-products are also obtained. Additionally, reactions with pure $Co(Ac)_2$, $Ni(Ac)_2$ and $Zn(Ac)_2$ were also conducted at 200, 300 and 400 °C and 25 MPa.

Hydrothermal reaction of $Fe(Ac)_2$ and the mixture of acetates took place at temperatures as low as 200 °C at 25 MPa and dark brown/black solids were obtained in all the cases. The PXD pattern of the hydrolysis product of pure $Fe(Ac)_2$ showed mainly a mixture of magnetite, Fe_3O_4 [JCPDS 19-0629] and some metallic Fe [JCPDS 06-0696] (Table 1).

Reactions of pure $Co(Ac)_2$, $Ni(Ac)_2$ and $Zn(Ac)_2$ were also conducted at 200, 300 and 400 °C and 25 MPa (not tabulated). Under flow conditions, reaction of $Co(Ac)_2$ gave a very light yellow/brown suspension. However, most of the solid in the suspension redissolved in the mother liquor within one day (80–60% estimated by UV) and a brown solid precipitated in low yield. The solution was decanted and the dry powder analysed, consisting mostly of CoO [JCPDS 09-0402] and, at 200 °C, minor peaks due to Co_3O_4 [JCPDS 09-0418]. Further *in-situ* studies will be needed to identify the reaction products, prior to dissolution.

Hydrothermal reactions of $Ni(Ac)_2$ were conducted at 200, 300 and 400 °C and 25 MPa. When the reaction was conducted at 200 °C, the reaction yield was relatively low (33% by UV) and insufficient solid was collected for analysis. At 300 °C, the reaction yield increased up to 85% by UV and the solid was identified as a mixture of NiO [JCPDS 22-1189 and 04-0835] and synthetic theophrastite, $Ni(OH)_2$ [JCPDS 14-0117]. At 400 °C, the $Ni(Ac)_2$ solution decomposed almost totally, although only incomplete dehydration of the nickel hydroxide

Table 3 Density,[23] ρ, ionic product, pK_w*,[29] and dielectric constant, ε,[28] of water and residence time of the mixture, t_R, at the conditions of the experiments

T/°C	P/MPa	ρ/g cm^{-3}	t_R/s	pK_w*	ε
200	25	0.882	25	11.16	35.7
300	25	0.743	21	11.14	21.6
400	25	0.166	5	19.44	2.4

was achieved. Hydrothermal reaction of $Zn(Ac)_2$ at 200, 300 and 400 °C and 25 MPa did not give ZnO. At the different temperatures, a slightly cloudy solution was obtained but it cleared rapidly.

For the majority of cobalt and nickel ferrites, as well as the mixed cobalt and nickel ferrites, dark brown/black powders were obtained with a single spinel PXD pattern very similar to that of pure magnetite (Table 2). For the cobalt ferrites, the spinel pattern was identified as cobalt iron oxide, $CoFe_2O_3$/Fe_3O_4·CoO [JCPDS 22-1086]. When the iron to cobalt molar ratio in the starting solution was 1 : 1 (run 6 in Table 2), apart from the cobalt ferrite [JCPDS 22-1086], very weak peaks due to CoO were identified [JCPDS 09-0402]. For the nickel ferrites, the spinel pattern matched that of a synthetic trevorite, $NiFe_2O_4$, and/or a nickel defective trevorite, $(Ni,Fe)Fe_2O_4$ [JCPDS 10-0325 and 23-1119, respectively] (runs 8–10 in Table 2). In some of the experiments conducted with Ni and Fe (runs 8, 10 and 11 in Table 2), minor peaks due to metallic Ni [JCPDS 04-0850] were found in the PXD pattern. The hydrolysis of the mixture of Zn(II) and Fe(II) acetates did not give a single phase material and a black solid containing a mixture of zinc ferrite [JCPDS 22-1012], metallic iron [JCPDS 06-0696] (weak) and magnetite [JCPDS 19-0629] (very weak) was obtained at all conditions (runs 14–16 in Table 2). Additionally, in some of the samples, PXD data revealed the presence of minor impurities, with very weak intensities, which could reflect the presence of very small amounts of a hydrated iron(III) oxide, $Fe_2O_3·H_2O$ [JCPDS 06-0696], or some unreacted starting material. Starting materials and $Fe_2O_3·H_2O$ seem to contaminate particularly the products of the reactions conducted at 200 °C and the decomposition products of the mixtures of Fe(II) and Zn(II) acetates.

PXD patterns of the different materials synthesised at 300 °C and 25 MPa are shown in Fig. 2. They are very similar, as

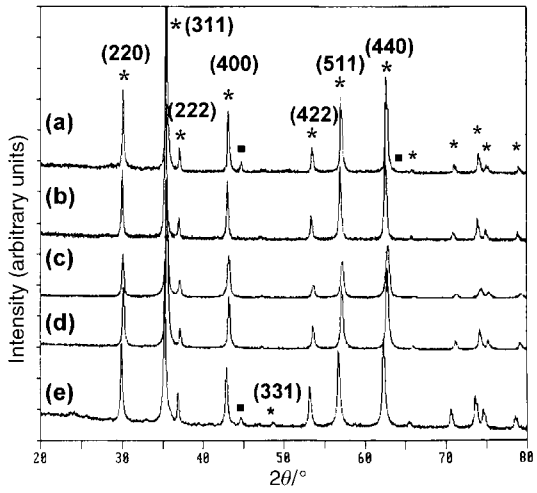

Fig. 2 Powder X-ray Diffraction (PXD) patterns of the hydrolysis products of the mixtures of Fe(II) and metal(II) acetates produced in the flow reactor at 300 °C and 25 MPa: (a) pure $Fe(Ac)_2$ (run 2), (b) 2 : 1 mixture of $Fe(Ac)_2$ and $Co(Ac)_2$ (run 5), (c) 2 : 1 mixture of $Fe(Ac)_2$ and $Ni(Ac)_2$ (run 9), (d) 2 : 0.5 : 0.5 mixture of $Fe(Ac)_2$, $Co(Ac)_2$ and $Ni(Ac)_2$ (run 12), (e) 2 : 1 mixture of $Fe(Ac)_2$ and $Zn(Ac)_2$ (run 15). Ferrite, MFe_2O_3 (*) and Fe (■) PXD peaks are indicated.

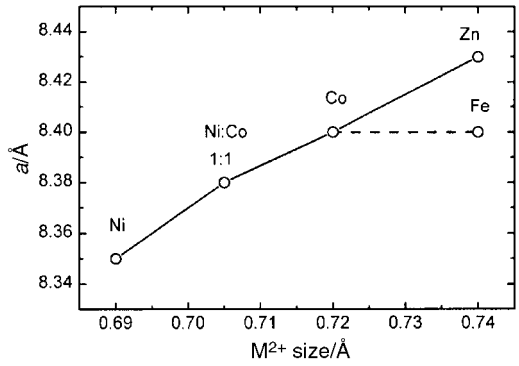

Fig. 3 Lattice parameter, a, of the ferrites, MFe_2O_3, produced in the flow reactor at 300 °C and 25 MPa, against ionic radius of the cation M^{2+}. The solid lines connecting the lattice parameters are drawn to aid visualisation.

expected, due to the small variation of ionic radii. The cell parameters of the different materials were obtained from the refinement of the PXD positions using a standard least squares fitting procedure. Fig. 3 shows the lattice parameters of the different spinels produced in the flow reactor at 300 °C and 25 MPa, plotted against the ionic radius of the M^{2+} cations.[24] For Co, Ni and Zn ferrites, the lattice parameters correlate with the size of the M^{2+} cation, which decreases from Zn to Ni. For plotting the data for the mixed Co and Ni ferrite, the average ionic radii of Co^{2+} and Ni^{2+} was used. The smaller the ionic radius, the smaller the lattice parameter. The cell parameters obtained for $CoFe_2O_4$ and Fe_3O_4 are very close so PXD data alone cannot prove incorporation of Co into the lattice. In this case, the ratio of the different metals was analysed by other techniques. AA analysis revealed a Fe : Co ratio in the bulk very close to the stoichiometric 2 : 1. EDX metal analysis confirmed the presence of Co in the sample. By contrast, although Zn^{2+} and Fe^{2+} have very similar ionic radii,[24] the lattice parameters of the corresponding ferrites were quite different. For this material, however, the amount of Zn incorporated into the structure according to AA and EDX analysis was much lower than expected. The differences observed between zinc ferrite and magnetite may be due to the different degree of inversion in the spinel lattice; zinc ferrite is a normal spinel whilst magnetite is an inverse. Very similar results were obtained at the different temperatures.

For the hydrolysis reactions of $Fe(Ac)_2$ and the mixture of acetates in water, no quantification of the reaction yield was made. In most cases, very dark brown or black suspensions were collected after the back-pressure regulator and visual inspection suggested high decomposition yields. Microanalysis of the samples, however, showed a high carbon content (Tables 1 and 2). This may be indicative of unreacted starting material left as a result of the method of drying. Up to 16% weight of carbon was found in some of the materials synthesised at the lowest reaction temperature. For experiment 6, which was conducted at 300 °C and 25 MPa with a Fe to Co ratio 1 : 1, a very high carbon content was found. This high carbon content could be attributed to unreacted $Co(Ac)_2$. In the reactions conducted at 400 °C, the solid separated more easily and the supernatant liquid remained almost clear and, although the carbon content was smaller, it was still appreciable in most cases. Possibly, this carbon content could be due, at least in part, to the presence of acetate groups attached to the surface of the precipitates. FT-IR spectra of the materials produced in the flow reactor showed bands due to acetate groups in all the samples. As expected, the intensity of these bands increased with the carbon content of the samples.

The relative amounts of the different metals in the ferrites determined by AA were, for the single ferrites of cobalt and

nickel, very close to those employed in the starting metal solutions, suggesting near quantitative decomposition of the starting materials. For the mixed Co/Ni ferrites, the Co content was close to that expected, but the Ni content was considerably higher than expected. At such a high Fe : Ni ratio, the Ni content determined by AA may well be an over-estimate, so the actual nickel content remains uncertain and the material is better represented as $Ni_xCo_{1-x}Fe_2O_4$. For the zinc ferrite experiments, the Zn content in the samples was clearly smaller than expected.

Discussion

Reaction mechanism

Adschiri *et al.*[15] have reported that the decomposition of most metal nitrates and other salts (*e.g.* sulfates) proceeds *via hydrolysis* to the hydroxides, followed by *dehydration* to the oxides (equations (i) and (ii))

(i) Hydrolysis step:

$$ML_x(aq) + xH_2O \rightarrow M(OH)_x(s) + xHL$$

(ii) Dehydration step:

$$M(OH)_x(s) \rightarrow M(O)_{x/2}(s) + x/2H_2O$$

Using a flow reactor, they showed that $Fe(NO_3)_3$ and $Fe_2(SO_4)_3$ hydrolysed and dehydrated at 400 °C and 35 MPa in scH_2O producing Fe_2O_3. Under the same conditions, the hydrolysis of $FeCl_2$ also yielded Fe_2O_3 although the additional oxidation step was not explained. However, under identical conditions, degradation of an iron(III) citrate complex, $Fe(NH_4)_2H(C_6H_5O_7)_2$, gave pure magnetite.[15,16] It was suggested that this may be the result of the partial reduction of Fe^{3+} cations by CO gas produced by thermal decomposition of the citrate.

A similar mechanism is expected for the decomposition of $Fe(Ac)_2$. However, for these systems, there is an additional oxidation step, which has to be considered. A possible reaction mechanism is proposed in Scheme 1 (reaction steps a to i).

When a solution of $Fe(Ac)_2$ is treated hydrothermally in the flow reactor, a suspension containing a mixture of Fe and Fe_3O_4 is obtained in the majority of cases. According to the mechanism proposed above, $Fe(Ac)_2$ hydrolyses, forming $Fe(OH)_2$ (step b in Scheme 1), which dehydrates further to give FeO (step f). However, FeO is not stable at temperatures below 575 °C[25] and disproportionates immediately, giving a mixture of Fe and Fe_3O_4 (step h) according to reaction (iii).

(iii) Disproportionation:

$$4FeO \rightarrow Fe + Fe_3O_4$$

In a solid state reaction, metastable FeO can be detected by quenching the reaction rapidly, a procedure which is not possible in solution.

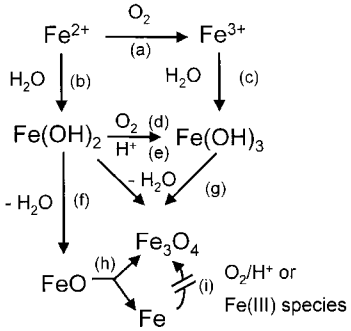

Scheme 1 Proposed mechanism for the decomposition of $Fe(Ac)_2$ in nc- and scH_2O.

Additionally, the direct oxidation of Fe^{2+} to Fe^{3+} in acidic solution or, more probably, the oxidation of the freshly precipitated $Fe(OH)_2$ could take place. Small amounts of O_2 in the water could easily oxidise the Fe(II) species. The standard redox potentials, E°, of the reaction with O_2 for Fe^{2+} (step a) and $Fe(OH)_2$ (step d) are 0.46 and 1.79 V, respectively.[24] Also, water can oxidise $Fe(OH)_2$ to $Fe(OH)_3$ (step e) generating H_2 ($E^\circ = 0.56$V).[24] Dehydration of a mixture of $Fe(OH)_2$ and $Fe(OH)_3$ would produce Fe_3O_4 (step g). The existence of Fe(II) ions in solution seems to play a crucial role in the formation of the spinel by formation of an intermediate complex hydroxide of Fe(II) and Fe(III) which prevents polymerization of $Fe(OH)_3$ and formation of Fe_2O_3.[1]

The above discussion has been made without considering temperature and pressure effects in the redox potentials. Although the pressure and temperature dependences of the redox potential at near-critical and supercritical conditions follow the usual thermodynamic relationships, an exact treatment is outside the scope of this paper and the standard redox potentials have been used to discuss the possible redox reactions.

The effect of temperature on the product distribution (relative amounts of Fe and Fe_3O_4) can be explained considering the reaction enthalpies. The standard enthalpies of the different dehydration reactions yielding FeO (step f) and Fe_3O_4 (step g) are 16.17 and −24.94 kJ mol^{-1}, respectively.[26] Whilst formation of FeO from $Fe(OH)_2$ (step f) is an endothermic process which is favoured at high temperatures, dehydration of the mixture of $Fe(OH)_2$ and $Fe(OH)_3$ to Fe_3O_4 (step g) is an exothermic process which becomes less important at higher temperatures. As a result, at 200 °C, the amount of metallic Fe in the product is almost negligible.

Another factor to consider is the residence time. For a fixed reactor volume, the residence time at 25 MPa decreases from 25 to 5 seconds as the temperature increases from 200 to 400 °C (Table 3). Longer residence times may allow re-oxidation of the metallic Fe by H^+, O_2 or Fe(III) species (step i).

When the same reaction was conducted in a batch reactor (3.3 ml) using a procedure similar to that described by Boix and Poliakoff[27] at 380 °C and 33 MPa for 1 hour, there was no evidence for formation of metallic iron and only pure Fe_3O_4 was obtained. The conditions were similar to those employed in the flow experiments apart from the pressure being slightly higher, but the reaction time in this case was much larger than those employed in the flow experiments of only a few seconds. In addition, in the batch experiments, the reactor was not purged with N_2. With longer reaction times and higher concentrations of O_2, metallic Fe formed from the disproportionation of FeO can be re-oxidised in H_2O giving Fe(II) or Fe(III) species, eventually producing Fe_3O_4 (step i).

Hydrothermal reactions of pure $Co(Ac)_2$, $Ni(Ac)_2$ and $Zn(Ac)_2$ were also conducted (not tabulated). As discussed before, the degree of hydrolysis and dehydration was different in the different metal acetates. $Co(Ac)_2$ hydrolysed very easily even at 200 °C, although most of the hydroxide/oxide which was formed re-dissolved in the mother liquor. In contrast to the Fe case, H_2O is not oxidising enough to oxidise Co(II) species and only O_2 can oxidise $Co(OH)_2$ to $Co(OH)_3$ ($E^\circ = 1.04$ V)[24] and, as a result, the main reaction product after dehydration was CoO. Decomposition of $Ni(Ac)_2$ occurred above 200 °C although in low yield, but it was almost complete at 300 and 400 °C and 25 MPa. Nevertheless, complete dehydration of the hydroxide was not achieved. The hydrothermal reaction of $Zn(Ac)_2$ at the different temperatures gave only a slightly cloudy solution, which cleared rapidly, suggesting the incipient formation of the hydroxides but only in very small amounts.

For the Ni and Co ferrites, as well as for the mixed Ni/Co ferrite, there was no evidence in the PXD pattern of any metallic Fe when the hydrolysis of the mixture of acetates was carried out in the flow reactor in nc- or scH_2O. In most of the

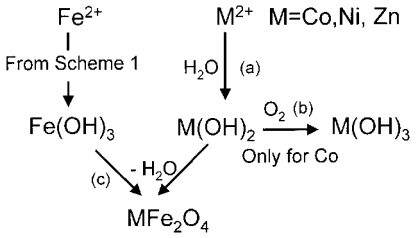

Scheme 2 Proposed mechanism for the decomposition of a mixture of $Fe(Ac)_2$ and different metal(II) acetates, $M(Ac)_2$, in nc- and scH_2O.

cases, a single ferrite pattern almost identical to that of pure magnetite was obtained. A similar mechanism to that described above is expected, involving precipitation of the corresponding hydroxides and subsequent dehydration, and is illustrated in Scheme 2 (reaction steps a to c). Oxidation of Fe(II) species, as well as of Co(II), is possible. Water can oxidise $Fe(OH)_2$ in absence of O_2 partly due to the lower solubility of the $Fe(OH)_3$. However, only O_2 could oxidise $Co(OH)_2$ (step b in Scheme 2). Oxidation of Ni(II) is, however, unlikely. PXD data show that dehydration of the mixed hydroxides $Fe(OH)_3$ and $M(OH)_2$ (M = Co, Ni or a mixture of Co and Ni) yields a single phase MFe_2O_4 in the majority of the cases (step c). For Co, if some oxidation of $Co(OH)_2$ did occur (step b), the material would be better represented by $[Co^{2+}{}_{1-x}Fe^{2+}{}_x][Co^{3+}{}_xFe^{3+}{}_{2-x}]O_4$ where x is the amount of Co^{3+} replacing Fe^{3+} in the spinel structure.

For some of the experiments conducted with $Fe(Ac)_2$ and $Ni(Ac)_2$, minor peaks due to metallic Ni were identified in the PXD. Oxidation of $Fe(OH)_2$ in water generates H_2 which could act as reducing agent for Ni(II) species. Fe or $Fe(OH)_2$ might also reduce Ni^{2+} during the course of the reaction.

PXD analysis of the product from the hydrothermal reaction of a mixture of Fe(II) and Zn(II) acetates at the different temperatures did not show a single phase material but a mixture of a zinc ferrite, metallic iron (weak) and magnetite (very weak). This seems to be the consequence of the different rates of hydrolysis of $Fe(Ac)_2$ and $Zn(Ac)_2$. $Fe(Ac)_2$ hydrolyses very rapidly (step b in Scheme 1), whilst hydrolysis of $Zn(Ac)_2$ (step a in Scheme 2) seems to be a much slower process. At a short time after the reactants have reached the mixing point, the concentration of $Zn(OH)_2$ is negligible compared to the concentration of iron hydroxides. As discussed above, dehydration of $Fe(OH)_2$ is fast giving FeO, which disproportionates to a mixture of magnetite and metallic iron. The mixture of $Fe(OH)_2$ and $Fe(OH)_3$ gives Fe_3O_4. Only after $Zn(Ac)_2$ has hydrolysed (step a in Scheme 2) does the mixture of $Fe(OH)_3$ and $Zn(OH)_2$ dehydrate to zinc ferrite (step c in Scheme 2). The intensity of the magnetite PXD peaks relative to that of metallic iron is smaller than those found in the decomposition of pure $Fe(Ac)_2$ under the same conditions (Fe_3O_4 in Fig. 2e is detected as a shoulder on the (311) "$ZnFe_2O_4$" peak). When only iron is present in the medium, there are two possible mechanisms for magnetite formation, as shown in Scheme 1; disproportionation of FeO (step h) or dehydration of Fe(II) and Fe(III) hydroxides (step g). When $Zn(OH)_2$ is present, the formation of the zinc ferrite by dehydration of the mixed hydroxides (step c in Scheme 2) seems to be more favourable than the dehydration of pure iron hydroxides (step g in Scheme 1). Therefore Fe_3O_4 would be produced mainly by disproportionation of FeO (step h in Scheme 1). As discussed before, thermodynamic arguments can rationalise the higher intensity of the metallic Fe peaks as the temperature increases. The Zn content in the samples, as analysed by AA and EDX, was smaller than expected, which suggests incomplete hydrolysis of $Zn(Ac)_2$ at the conditions of the experiments. The amount of Zn in the samples appears to be largely independent of the experimental conditions.

To explore the effect of adding O_2 in these reactions, preliminary experiments were conducted replacing the pure H_2O stream by a 0.1 M H_2O_2 solution. H_2O_2 decomposes thermally inside the pre-heater generating O_2. The addition of O_2 to the mixture of $Fe(Ac)_2$ and $Co(Ac)_2$ yielded complex mixtures with no single phase materials. Experiments with H_2O_2 gave, at 300 °C and 25 MPa, a product mixture, which appears to be similar to that obtained by Holm and Teja in their flow reactor.[3] They generated a mixture of hydroxides by precipitation of a mixture of $Fe(NO_3)_3$ and $Co(NO_3)_2$ with NaOH, which was then dehydrated at 350 °C and 23 MPa. Further experiments would be needed to unravel our reactions with H_2O_2 and to identify the products fully.

We have attempted to relate the physical properties of the solvents with the reaction mechanism. Table 3 shows literature values for the density,[23] ρ, dielectric constant,[28] ε, and self-dissociation constant,[29] pK_w^*, of pure water at the experimental conditions. Residence times, t_R, are also indicated. The *hydrolysis step (i)* is favoured when the dielectric constant, ε, of water is low and when the ionic product, K_w^*, is high. ε decreases with ρ but K_w^* is a maximum in the near critical region (although K_w^* depends on ρ, self-dissociation of H_2O is an endothermic process). The *dehydration step (ii)* is preferred at higher temperature and it is easier with small particle sizes. The *oxidation reaction* does not seem to be strongly affected by

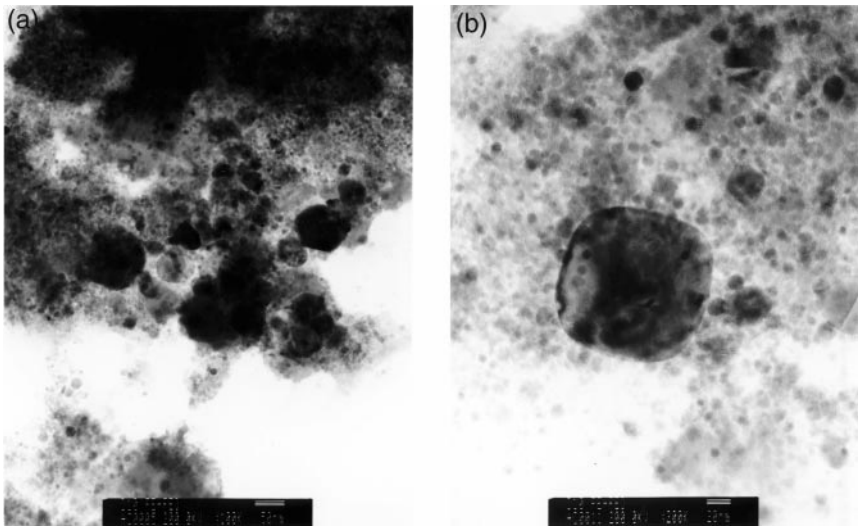

Fig. 4 Transmission Electron Micrographs (TEM) showing the decomposition product of pure $Fe(Ac)_2$ in the flow reactor at 300 °C and 25 MPa (run 2): (a) bar = 50 nm, (b) bar = 20 nm. Very small particles between 5–10 nm are clearly visible jointly with few larger particles between 80–100 cm.

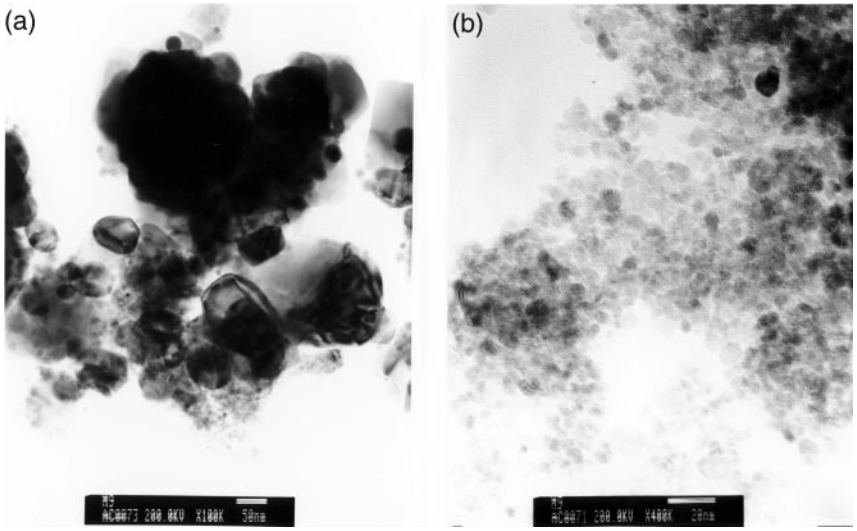

Fig. 5 Transmission Electron Micrographs (TEM) showing the decomposition product of pure $Fe(Ac)_2$ in the flow reactor at 400 °C and 25 MPa (run 3): (a) bar = 50 nm, (b) bar = 20 nm. Large particles (up to 100 nm) and smaller ones (5 nm) are observed in the micrograph. The tiny particles in (b) are smaller that those produced at 300 °C and 25 MPa (Fig. 4b).

temperature and pressure. Although the residence time decreases at 400 °C, the low dielectric constant of the medium induces faster saturation and dehydration and, as a result, the reaction yield increases.

Morphology

Particle size was estimated from the broadening of the PXD peaks according to the Scherrer equation. Large differences were observed among the estimates obtained from the different PXD reflections. For comparative purposes, the size estimated from the line-width of the (440) reflection was chosen as representative and is given in Tables 1 and 2. This peak was quite intense and did not overlap with other PXD peaks when more than one phase was identified.

Particle sizes in Tables 1 and 2 appear to increase, in most of the cases, with the reaction temperature, from 200 to 400 °C. However, the particle sizes of the materials produced at 300 °C were larger or smaller that those obtained at 200 °C, and no definitive trend was found. Increasing the reaction temperature from 300 to 400 °C increased the particle size in all the materials apart from the Ni/Co mixed ferrite. In this case PXD peaks of the material produced at 400 °C (run 13) were broader than those obtained at 300 °C (run 12) and, accordingly, the estimated particle sizes were smaller. A decrease in the particle size of the materials has been previously reported[30,31] when the experimental conditions change from nc- to scH_2O. This effect has been explained by a higher degree of super-saturation under supercritical conditions due to the lower solvating power of the medium, which induces faster nucleation and prevents crystal growth.

Additionally, selected samples were analysed by TEM, which revealed a "bimodal" particle size distribution: in every case small particles of less than 10 nm and larger aggregates of up to 100 nm. The high crystallinity of the materials was confirmed by the electron diffraction patterns obtained from the TEM. The pattern consisted of a number of concentric rings due to the random orientation of the small crystalline particles and some discrete spots from the bigger particles.

The actual particle sizes revealed by TEM do not compare well with those estimated using the Scherrer equation, Tables 1 and 2. The size estimated by the PXD width should therefore be considered as an average. The complexity of the reaction mechanism may well be responsible of the broad particle size distribution.

TEM pictures of the decomposition product of pure $Fe(Ac)_2$ at 300 °C and 25 MPa (run 2) are shown in Fig. 4a and b, where two different particle sizes are clearly visible; small spherical particles between 5 and 10 nm and fewer larger particles between 80–100 nm in diameter. Increasing the reaction temperature up to 400 °C (run 3) seems to decrease slightly the size of the small particles but, conversely, the number of larger particles increases as well as their size, as is shown in Fig. 5a and b respectively. In both cases, the material consists of a mixture of Fe_3O_4 with some Fe. However, a distinct morphology characteristic of each of the products has not been found, and it is not likely that the small and large particles correspond to different materials. The "bimodal" particle size distribution may merely reflect two different particle growth mechanisms.

TEM pictures of the Co ferrite and the Co/Ni mixed ferrite obtained at 300 °C and 25 MPa (runs 5 and 12) are shown in Fig. 6 and 7, respectively. The materials look very similar to that shown in Fig. 4, with very small particles and fewer larger ones.

For the Co ferrite sample (run 5), EDX analysis was conducted on different areas, focusing on large and small particles, respectively. The data revealed some heterogeneity in

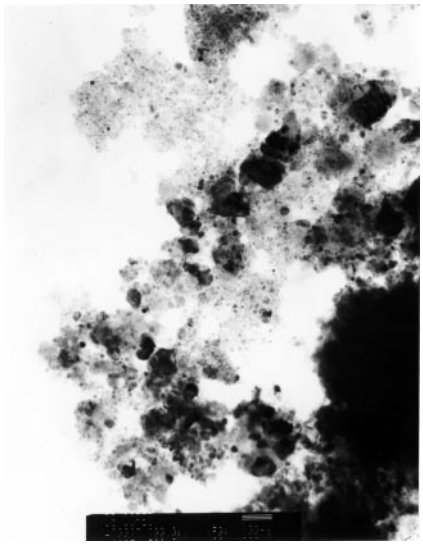

Fig. 6 Transmission Electron Micrograph (TEM) showing the decomposition product of a 2 : 1 mixture of $Fe(Ac)_2$ and $Co(Ac)_2$ in the flow reactor at 300 °C and 25 MPa (run 5). Bar = 100 nm. The material looks very similar to that shown in Fig. 4a.

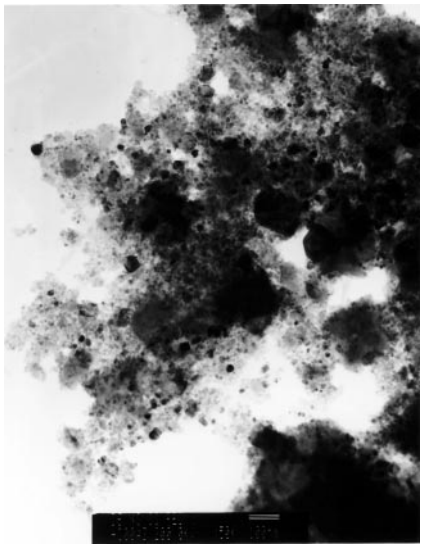

Fig. 7 Transmission Electron Micrograph (TEM) showing the decomposition product of a 2 : 0.5 : 0.5 mixture of $Fe(Ac)_2$, $Co(Ac)_2$ and $Ni(Ac)_2$ in the flow reactor at 300 °C and 25 MPa (run 12). Bar = 100 nm. The material looks very similar to those shown in Fig. 4a and 6.

the composition of the sample which appeared to be related to the morphology of the material with Co : Fe ratios varying between 2 : 0.4 and 2 : 1. Larger particles showed a higher Co content very close to the stoichiometric. Analysis of the composition of the smaller particles revealed, however, lower Co contents than those expected. No areas of excess Co content were identified.

TEM of the material obtained from the decomposition of the 2 : 1 mixture of $Fe(Ac)_2$ and $Zn(Ac)_2$ (run 15) are shown in Fig. 8a and b. The pictures show a broad particle size distribution. The material is composed of small particles of 10–15 nm size and larger aggregates of up to 100 nm. The small particles are spherical in shape, whilst the larger particles appeared more crystalline, with a rhomboidal or polyhedral shape.

EDX analysis was performed on the hydrolysis product of the mixture of $Fe(Ac)_2$ and $Zn(Ac)_2$ (run 15). The measured Fe : Zn ratios were between 2 : 0.4 and 2 : 0.5 for the different areas analysed. From the EDX analysis, no single Fe and Fe_3O_4 particles (evident in the PXD) were identified. Any attempt to relate morphology and composition was unsuccessful due to the difficulty of finding isolated particles with different morphologies.

The amount of Fe present in the samples determined by EDX was always larger than those obtained by AA. Fluorescence or back-scattered electron excitation of X-rays from the specimen holder and microscope column in the EDX analysis could explain the differences found between the techniques. When elements of similar atomic number are presents in the sample, fluorescence can be quite significant. The fluorescence effect would give rise to more of the lower energy X-rays (in this case Fe) than would be expected.[32]

Conclusions

In this work, we have reported the continuous synthesis of nano-particulate magnetic spinel type oxides in near-critical and supercritical water. By combining hydrothermal synthesis and partial oxidation, we have been able to synthesise Fe_3O_4, $CoFe_2O_4$, $NiFe_2O_4$, "$ZnFe_2O_4$" and $Ni_xCo_{1-x}Fe_2O_4$, by the simultaneous hydrolysis and partial oxidation of the corresponding metal acetates in ncH_2O and scH_2O. The process is simple and clean and requires neither the addition of bases to the system nor the use of very high reaction temperatures. Relatively large amounts of material (up to 7 g h^{-1}) can be produced quickly and safely in a small reaction volume. The effects of temperature and residence time have been investigated, which has led to a possible reaction mechanism involving several redox processes. TEM examination of the samples showed a material composed of very small particles of *ca.* 10 nm with fewer larger particles of up to 100 nm. The nature of the crystal growth is not yet understood. A complex reaction mechanism may be responsible for the morphology.

Acknowledgements

We gratefully acknowledge the financial support of the EPSRC Grant no. GR/N06892, Clean Technology Fellowships and TMR research network Superclean Chemistry-2 Contract No. ERBFMRXCT970104. We thank M. Guyler and J. Green (Atomic Absorption), N. Bock (TEM pictures and EDX analysis) and T. R. Spencer (Microanalyses) for technical support. We thank Drs. J. A. Darr, A. A. Galkin, J. R. Hyde and D. H. Gregory for assistance/discussion of the manuscript.

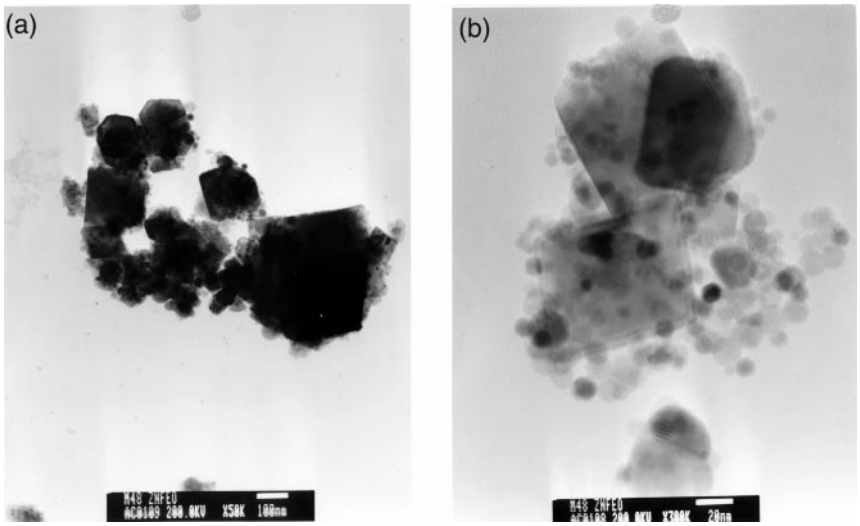

Fig. 8 Transmission Electron Micrographs (TEM) showing the decomposition product of a 2 : 1 mixture of $Fe(Ac)_2$ and $Zn(Ac)_2$ in the flow reactor at 300 °C and 25 MPa (run 15): (a) bar = 100 nm, (b) bar = 20 nm. The micrographs show a broad particle size distribution where the larger particles have a rhomboidal or polyhedral shape.

References

1 T. Kodama, Y. Wada, T. Yamamoto, M. Tsuji and Y. Tamaura, *J. Mater. Chem.*, 1995, **5**, 1413.
2 Y. Okano and T. Nakamura, *Colloids Surf. A: Physicochem. Eng. Aspects*, 1998, **139**, 279.
3 L. J. Holm and A. S. Teja, *5th International Symposium on Supercritical Fluids, Atlanta, Georgia, USA*, 2000.
4 S. Smit and H. P. J. Wijn, *Ferrites*, ed. P. T. Library, N.V. Philips' Gloeilampenfabrieken, 1959.
5 S. Hirano, T. Yogo, K. Kikuta, E. Asai, K. Sugiyama and H. Yamamoto, *J. Am. Ceram. Soc.*, 1993, **76**, 1788.
6 J. F. Hochepied, P. Bonville and M. P. Pileni, *J. Phys. Chem. B*, 2000, **104**, 905.
7 M. Kiyama, *Bull. Chem. Soc. Jpn.*, 1978, **51**, 134.
8 A. R. Gainsford, M. J. Sisley and T. W. Swaddle, *Can. J. Chem.*, 1975, **53**, 12.
9 H. Kumazawa, K. Oki, H. M. Cho and E. Sada, *Chem. Eng. Commun.*, 1992, **115**, 25.
10 G. W. Morey and P. Niggli, *J. Am. Chem. Soc.*, 1913, **35**, 1086.
11 A. Rabenau, *Angew. Chem., Int. Ed. Engl.*, 1985, **24**, 1026.
12 T. Adschiri, K. Kanazawa and K. Arai, *J. Am. Ceram. Soc.*, 1992, **75**, 2615.
13 J. A. Darr and M. Poliakoff, *Chem. Rev.*, 1999, **99**, 495.
14 A. Cabanas, J. A. Darr, T. Ilkenhans and M. Poliakoff, *6th Meeting on Supercritical Fluids, Nottingham, England 1999*, ed. M. Poliakoff, S. M. Howdle and M. W. George, ISASF, Nancy, 1999.
15 T. Adschiri, K. Kanazawa and K. Arai, *J. Am. Ceram. Soc.*, 1992, **75**, 1019.
16 T. Adschiri, S. Yamane, S. Onai and K. Arai, *3rd Int. Symp. on Supercritical Fluids, Strasbourg, France*, 1994.
17 L. Diamandescu, D. Mihaila-Tarabasanu, N. Popescu-pogrion, A. Totovina and I. Bibicu, *Ceram. Int.*, 1999, **25**, 689.
18 D. Chen and R. Xu, *Mater. Res. Bull.*, 1998, **33**, 1015.
19 H. Kumazawa, H. M. Cho and E. Sada, *J. Mater. Sci.*, 1993, **28**, 5247.
20 Y. Hakuta, T. Adschiri, T. Suzuki, T. Chida, K. Seino and K. Arai, *J. Am. Ceram. Soc.*, 1998, **81**, 2461.
21 A. Cabanas, J. A. Darr, E. Lester and M. Poliakoff, *Chem. Commun.*, 2000, 901.
22 A. Cabañas, J. A. Darr, E. Lester and M. Poliakoff, *J. Mater. Chem.*, 2001, **11**, 561.
23 E. Schmidt, *Properties of Water and Steam in SI-Units*, Springer-Verlag, Berlin, 1969.
24 *CRC Handbook of Chemistry and Physics*, ed. R. C. Weast, CRC Press, Boca Raton, FL, 1972.
25 N. N. Greenwood and A. Earnshaw, *Chemistry of the Elements*, Butterworth-Heinemann, London, 1997.
26 M. W. Chase Jr., *NIST-JANAF Thermochemical Tables*, ACS, Washington DC, 1998.
27 C. Boix and M. Poliakoff, *J. Chem. Soc., Perkin Trans. 1*, 1999, 1487.
28 M. Uematsu and E. U. Franck, *J. Phys. Chem. Ref. Data*, 1980, **9**, 1291.
29 W. L. Marshall and E. U. Franck, *J. Phys. Chem. Ref. Data*, 1981, **10**, 295.
30 Y. Hakuta, S. Onai, S. Terayama, T. Adschiri and K. Arai, *J. Mater. Sci. Lett.*, 1998, **17**, 1211.
31 T. Adschiri, *5th International Symposium on Supercritical Fluids, Atlanta, Georgia, USA*, 2000.
32 P. J. Goodhew and F. J. Humphrey, *Electron Microscopy and Analysis*, Taylor & Francis, London, 1988.